A Highly Efficient and Self-Stabilizing Metallic-Glass Catalyst for Electrochemical Hydrogen Generation

Yuan Chao Hu, Yi Zhi Wang, Rui Su, Cheng Rong Cao, Fan Li, Chun Wen Sun,* Yong Yang, Peng Fei Guan,* Da Wei Ding, Zhong Lin Wang, and Wei Hua Wang*

Hydrogen is one of the most promising and appealing alternative energy resources of fossil fuels to tackle the current energy crisis and environmental issues.[1] An economical routine for hydrogen generation is electrochemical water splitting or hydrogen evolution reaction (HER).[2–4] To render HER with high efficiency, highly active and durable electrocatalysts are of paramount importance. Although platinum (Pt)-based materials are found to be the most efficient for commercial electrocatalysts, the high cost and scarcity of Pt seriously impede its widespread applications. Additionally, researchers have developed numerous alternative catalysts for HER, such as metal oxides, carbides, sulfides, and their combinations with graphitic nanocarbons, etc.[4–6] In principle, these catalysts are crystalline and their electrochemical performance is intrinsically related to their crystal structures.[7] Besides the obstacle of the complex chemical synthesis processes, they cannot achieve both high activity and durability comparable to Pt-based alloys. Challenges still remain on how to improve both the electrocatalytic activity and durability of a catalyst for HER. Amorphous materials were also suggested to be active

catalysts for HER.[8–10] However, being best known for their superior mechanical properties, amorphous alloys or metallic glasses (MGs) have attracted intensive interests as structural materials rather than for functional applications.[11] Recently, through thermoplastic forming, Schroers and co-workers demonstrated the effectiveness of nanostructured MGs for electrochemical reactions.[8,12,13] Zhao et al.[14] and Yang et al.[15] also investigated the catalytic properties of MG nanoparticles and thin film for methanol electrooxidation and oxygen reduction reactions, respectively. Nevertheless, the application of MGs for HER is still blank. In this study, we report a multicomponent $Pd_{40}Ni_{10}Cu_{30}P_{20}$ MG catalyst, which not only exhibits excellent electrocatalytic activity but also possesses unique self-stabilizing catalytic performance over a long-cycling life. Such superior features of the amorphous catalyst originate from the self-optimized active sites, arising from the intrinsic chemical heterogeneity and the selective dealloying of elements on the multicompositional disordered surface, which uncover a new mechanism for improving the durability of catalysts.

The $Pd_{40}Ni_{10}Cu_{30}P_{20}$ alloy, one of the best known metallic-glass-formers,[16] was fabricated by arc melting and single-roll melt-spinning techniques in ribbons (Supporting Information). X-ray diffraction, differential scanning calorimetry, and high-resolution transmission electron microscopy analyses verify the amorphous structure of the ribbons (Figure S1, Supporting Information). A standard three-electrode configuration was used to evaluate the electrocatalytic performance of the disordered ribbon for HER in 0.5 M H_2SO_4 electrolyte. For comparison, a commercially available Pt/C (10 wt% Pt, Alfa Aesar) was also tested under the same conditions. To be convenient, all potentials in this study are referenced to the reversible hydrogen electrode (RHE). According to the polarization curves shown in **Figure 1**a,b, the overpotential of the $Pd_{40}Ni_{10}Cu_{30}P_{20}$ ribbon is only 76 mV driving a current density of $j = 10$ mA cm^{-2} after 10 000 cyclic voltammogram (CV) cycles in the potential range of ≈0.3 V to 0.1 V (vs RHE) at a scan rate of 100 mV s^{-1}, while the potential of the commercial Pt/C catalyst reaches 108 mV at the same condition. Therefore, the HER performance of MG is superior to the Pt/C catalyst, especially in terms of the long-term activity. After 10 000 CV cycles, like other crystalline catalysts, the electrocatalytic activity of Pt/C degrades seriously (see below); in sharp contrast, that of the MG exhibits an opposite trend. The onset potential of the MG, herein defined as the potential at a current density of $j = 0.6$ mA cm^{-2}, initially reaches the value 25 mV, comparable to 15 mV of Pt/C, as illustrated in Figure 1c. It is noteworthy that, when the onset potential of Pt/C grows to about 35 mV after 10 000 CV cycles, the quantity of the MG decreases to

Y. C. Hu, C. R. Cao, D. W. Ding, Prof. W. H. Wang
Institute of Physics
Chinese Academy of Sciences
Beijing 100190, China
E-mail: whw@iphy.ac.cn
Y. C. Hu, Dr. Y. Yang
Centre for Advanced Structural Materials
Department of Mechanical and Biomedical Engineering
City University of Hong Kong
Hong Kong, China
Y. Z. Wang, Prof. C. W. Sun, Prof. Z. L. Wang
Beijing Institute of Nanoenergy and Nanosystems
Chinese Academy of Sciences
National Center for Nanoscience and Technology (NCNST)
Beijing 100083, China
E-mail: sunchunwen@binn.cas.cn
Y. Z. Wang, Prof. F. Li
College of Environmental and Energy Engineering
Beijing University of Technology
Beijing 100124, China
Dr. R. Su, Prof. P. F. Guan
Beijing Computational Science Research Center
Beijing 100193, China
E-mail: pguan@csrc.ac.cn
Prof. Z. L. Wang
School of Material Science and Engineering
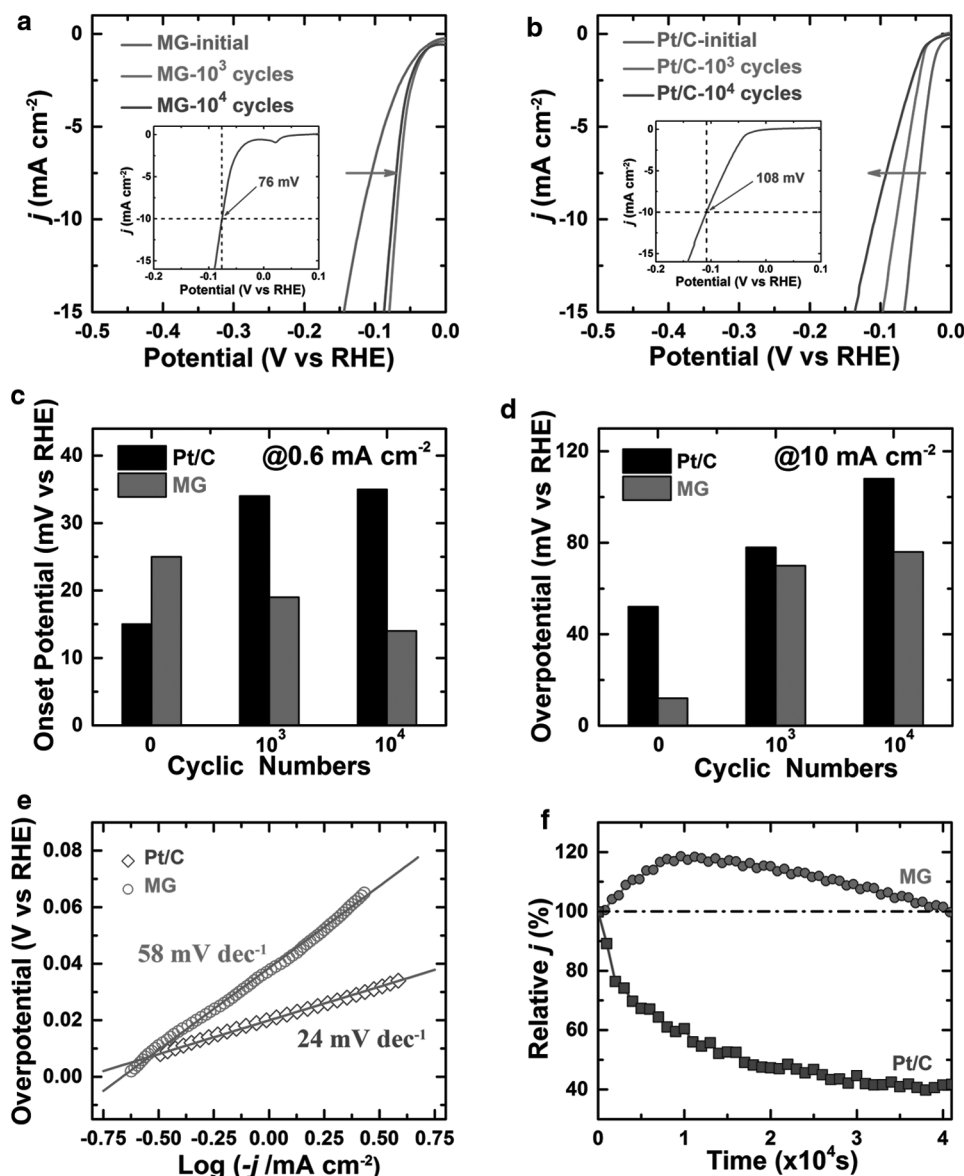Georgia Institute of Technology
Atlanta, GA 30332-0245, USA

COMMUNICATION

Figure 1. a,b) Polarization curves of the MG catalyst (a) and the 10 wt% Pt/C (b) in 0.5 M H_2SO_4 after 0, 1000, and 10 000 CV cycles. The insets show the overpotential at 10 mA cm^{-2} after 10 000 cycles. The arrows indicate the evolution trends of the curves. c,d) Comparisons of the onset potential at 0.6 mA cm^{-2} and the overpotential driving 10 mA cm^{-2} with increasing cyclic number. e) Tafel plots obtained from the polarization curves. f) Variations of the percentages of initial current at 300 mV versus time.

14 mV. This behavior indicates that Pt/C loses activity during the long time CV test, but the activity of the MG is somehow self-improved. Additionally, as depicted in Figure 1d, the overpotential of the MG catalyst driving the current density of 10 mA cm^{-2} stays at about 70 mV after 10 000 cycles, while that of Pt/C increases rapidly to above 100 mV.

Tafel slope is an intrinsic property of electrocatalysts for the hydrogen evolution reaction (HRE) and provides important clues to elucidate the HER pathways. To achieve this value, Tafel plots were fitted to the Tafel equation, $\eta = b \log(j) + a$, where η is the overpotential, b is the Tafel slope, and j is the current density (Figure 1e). The MG exhibits a small Tafel slope of 58 mV dec^{-1}, indicating that the hydrogen production on the amorphous catalyst surface possibly proceeds via

the Volumer–Heyrovsky mechanism. This value is much lower than many reported catalysts (**Figure 2** and Table S1, Supporting Information). The exchange current density (j_0) of the amorphous catalyst extrapolated from the Tafel plot is as high as 0.217 mA cm^{-2}, much larger than that of the Pt/C catalyst ($\approx$0.146) and many previously developed electrocatalysts.[5,17] The large j_0 indicates a large supplied current at very low overpotential and the activation of the overall reaction is much easier. These results all demonstrate the excellent HER electrochemical activity and kinetic property of the MG catalyst, being compared to other catalysts hitherto reported.

Long-term stability is also vital for HER catalysts. As aforementioned in Figure 1a,c, the electrochemical activity of the MG catalyst after 10 000 cycles is even better than the initial
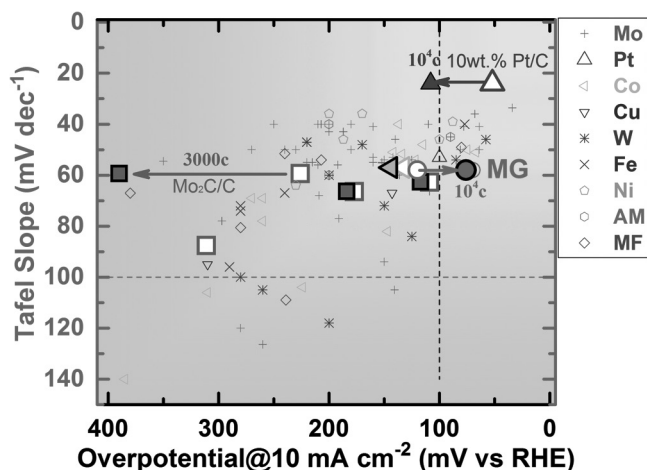
Figure 2. Tafel slop versus overpotential at 10 mA cm^{-2} for more than 100 kinds of catalysts (e.g., Mo-, Co-based catalysts, etc.) for HER. AM and MF represent previously reported inorganic amorphous materials and metal-free catalysts, respectively. A good catalyst should have both low Tafel slope and the overpotential (top right area), as also indicated by the dash lines. The arrows from the open to filled symbols denote changes in the performance after different cycle numbers (c). For instance, after 10 000 cycles (10^4 c), the activity of Pt/C degrades but that of the MG improves. This summary indicates the high performance of the MG for HER over many crystalline catalysts.

state, illustrating excellent durability of the amorphous catalyst. Furthermore, the durability of the amorphous $Pd_{40}Ni_{10}Cu_{30}P_{20}$ ribbon was assessed by electrolysis at a static potential -0.3 V (vs RHE) with a chronoamperometry measurement. 10 wt% Pt/C was also tested for comparison. Impressively, the current density of the MG increases at the early stage of the electrochemical testing and reaches the maximum around 10 000 s. After that, the efficiency declines slowly (Figure 1f)[12] and still retains 100% after 40 000 s. Contrarily, the efficiency of Pt/C plunges abruptly and remains only 40% of the initial value after 40 000 s test. Here we would like to emphasize that even after 100 000 s, the catalyst is still more robust than the Pt/C catalyst and keeps the amorphous nature (Figure S1a, Supporting Information). These results demonstrate that the MG possesses not only superior electrocatalytic activity in acidic solutions for HER but also unprecedented excellent durability.

To further highlight the superior overall performance of the amorphous catalyst, we compare the Tafel slope and the overpotential driving 10 mA cm^{-2} of the amorphous $Pd_{40}Ni_{10}Cu_{30}P_{20}$ catalyst with those of more than 100 kinds of electrocatalysts reported previously for HER in acidic media (Figure 2 and Table S1, Supporting Information). Obviously, Mo, Co, and Ni-based catalysts are the most widely studied ones for HER; meanwhile, they are also usually combined with highly conductive carbon nanotubes or graphene to enhance the activity. It can be seen that $Pd_{40}Ni_{10}Cu_{30}P_{20}$ MG belongs to the best performing catalyst group, with both Tafel slope and the overpotential lower than 100. Comparatively, its activity toward HER is more efficient than many crystalline catalysts, such as supported $[Mo_3S_{13}]^{2-}$ nanoclusters,[18] metal-free C_3N_4/N-doped graphene,[19] and is also better than some other inorganic amorphous catalysts.[9,20] More importantly, as indicated by the arrows in Figure 2, the effectiveness of MG increases at first,

being opposite to the rapid degradation of the efficacy in crystal catalysts. This intriguing and abnormal property of the MG catalyst may also suggest a new mechanism to improve the electrocatalytic activity for HER.

In order to gain insights in the impressive durability of the MG catalyst, X-ray photoelectron spectroscopy (XPS) was performed to probe the variations of the composition and valence state on the surface of the amorphous ribbon during the electrolysis test. **Figure 3**a shows the spectra of Pd 3d, which indicates that metallic Pd (Pd^0) dominates in the fresh sample, while electrocatalytic active ion (Pd^{2+}) appears over the course of the electrochemical test (see below). Conversely, the Cu 2p spectra show oxidized state Cu^{1+}and Cu^{2+} on the surface (Figure 3b), consistent with the previous results.[8] The oxidized state of Cu/Ni in the fresh sample is due to the strong covalent-like bonding between Cu/Ni and P which induces the charge transfer from Cu/Ni to P.[21] However, these oxidized states disappear after HER disposal and only metallic Cu^0 remains on the surface. Regarding to the surface composition change (Table S2, Supporting Information), it is distinct that selective dealloying happens during the electrochemical testing process, due to the electronegativity difference. After 100 000 s, Ni entirely disappears from the surface of the amorphous ribbon; meanwhile, the magnitudes of Cu and P decrease to different degrees. As a result, the surface becomes Pd abundant. This compositional change is crucial to understanding the high performance of the MG for HER, as discussed below.

Theoretically, the two processes of HER, hydrogen adsorption and desorption, can be summarized in a three-state diagram, which contains an initial state of H$^+$ + e$^-$, an intermediate state of H$_{ads}$ (where ads indicates an adsorbed state) and a final product of 1/2 H$_2$. To maintain a high catalytic activity, the hydrogen should not bind to the catalyst surface too strong so that both of the processes are fast. Such requirements indicate catalysts owing a close to thermoneutral free energy of adsorbed H ($\Delta G_H \approx 0$ eV) have a higher activity for HER.[22] Based on the systematical density functional theory calculations of two hundreds of absorption sites (Supporting Information), the distribution of ΔG_H on amorphous $Pd_{40}Ni_{10}Cu_{30}P_{20}$ surface is presented in Figure 3c (also see Figure S2, Supporting Information, for exemplified sites). Obviously, the MG surface exhibits a wider distribution of ΔG_H than the crystalline surfaces due to the intrinsic chemical heterogeneity of amorphous materials that provides abundant types of active sites (Figure S3, Supporting Information).[23] It presents a broad peak localized around $\Delta G_H \approx 0$ eV and suggests high activity for HER which is consistent with the experimental results. According to the element analysis of these absorption sites, it was found that ΔG_H is strongly dependent on the local chemical environment. We calculated the statistical atomic percent of each element for various sites with different ΔG_H. The histograms of the atomic percent of different elements are shown in Figure 3d. It presents that the absolute value of ΔG_H ($|\Delta G_H|$) approaches 0 as the atomic percent of Ni decreases. It implies that the experimental result in Figure 1f which shows the activity of HER becomes higher at the early stage of the electrochemical testing can be attributed to the self-optimization of active sites due to the selective dealloying of Ni element. Since these sites with $|\Delta G_H| < 0.1$ eV all contain Cu element, it suggests that the local
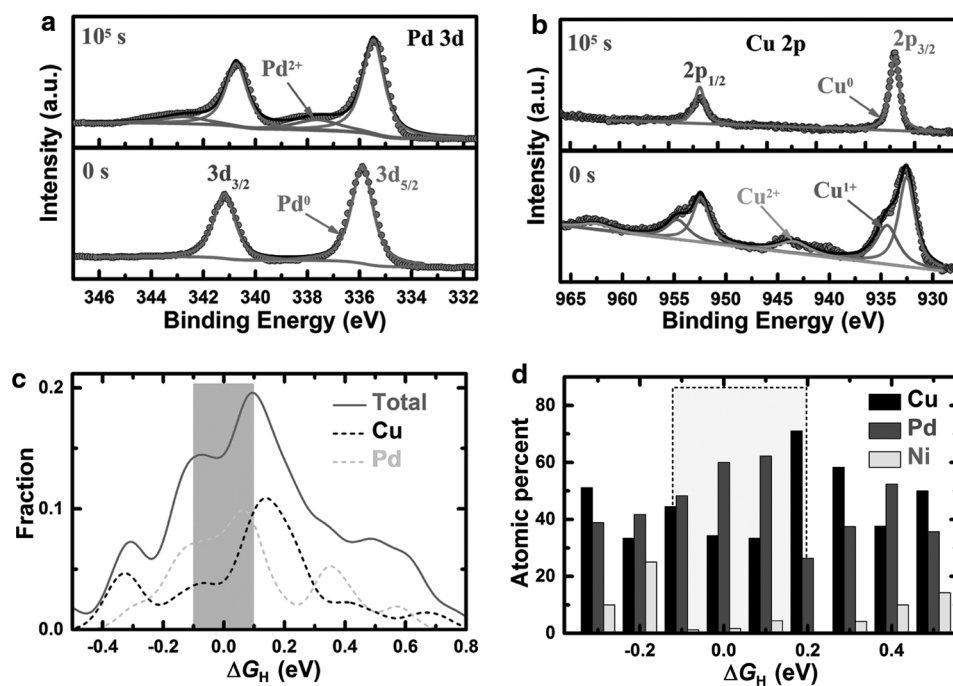
COMMUNICATION

Figure 3. a) Pd 3d spectra indicate a metallic state of Pd initially but with +2 oxidation state after 100 000 s test. b) The spectra of Cu 2p in the fresh sample can be fitted with three doublets ($2p_{3/2}$ and $2p_{1/2}$) of Cu^0, Cu^{1+}, and Cu^{2+}, while only metallic Cu doublet remains after electrochemical testing. c) Free energy ΔG_H distribution of HER on different adsorption sites on the amorphous surface. d) Chemical environment of adsorption sites with various ΔG_H.

Pd and Cu atomic order on the MG surface plays an important role for high HER activity. Therefore, as the selective dealloying of Cu also happens, the HER activity of the MG surface decreases later, consistent with the experimental results in Figure 1f. However, the complex chemical environment makes the decay of HER activity of amorphous surface much slower than crystalline surface with simple chemical environment.

To further illustrate the origin of the superior HER activity and the effect of the local chemical environment, the projected density of states (PDOS) of the selected Pd and Cu site with $\Delta G_H \approx 0$ eV was calculated and shown in Figure S2 (Supporting Information). The d-orbitals of Pd and Cu atoms show a main d-band peak at around −2.5 eV with two disorder-induced band tails from −6.0 to −4.5 eV and from −1.0 to 0 eV (inset). The bonding of H atom with the substrate is mostly contributed by the hybridization of H 1s orbital and the d band tails. Thus the bonding mechanism is different from the case on a crystal surface where the d orbital of the metal atoms is more extended in space. When compared to Cu, the PDOS of Pd atom shows a stronger binding with H atom due to the larger DOS values in the band tail. The differential charge pattern also confirms a larger charge transfer from H to Pd atom (Figure S2, Supporting Information). Due to the different binding energy between the H–Cu and H–Pd pairs, the change of ΔG_H can be understood from a competing mechanism between Cu and Pd atoms. Therefore, the theoretical calculations suggest that the excellent electrocatalytic activity of the MG ribbon for HER originates from the abundance of the active sites induced by the special electronic structure on the amorphous surface. Nevertheless, although Ni and P have less contribution to the HER

active sites, they play important roles in the glass formation (Supporting Information).

According to the XPS measurements, different degrees of selective dealloying on the surface happen to Cu and Ni during the HER, which, however, proceeds without changing the amorphous nature (Figure S1a, Supporting Information). Furthermore, Ni completely dissolves from the surface after 100 000 s, whereas Pd turns to be enriched (Table S2, Supporting Information). The initial improvement of the electrocatalytic activity observed in Figure 1a,f is attributed to the rapid increase of the active sites of localized Pd and Cu element groups induced by strongly dealloying of Ni. After an intermediate period, further dealloying of Ni and Cu changes the local chemical environment and atomic coordination; hence, the Pd and Cu sites start to decrease, resulting in gradual degradation of the performance. However, unlike the crystalline surface with single type of active site, the abundant types of active sites make the decay of electrochemical activity much slower. Therefore, the underlying mechanism of the electrocatalytic activity and self-stability of the amorphous $Pd_{40}Ni_{10}Cu_{30}P_{20}$ catalyst could be understood from the combining effects of external selective dealloying and the self-optimized activity sites with special electronic structure.

In summary, we prepared the $Pd_{40}Ni_{10}Cu_{30}P_{20}$ ribbons with stable amorphous structure by simple and scalable physical metallurgy techniques and studied its feasibility as a highly efficient electrocatalyst for water splitting. The amorphous catalyst exhibits higher catalytic activity for HER in the acidic electrolyte with the anomalous self-stability behaviors. The efficiency of the MG catalyst self-improves at the early stage of the electrochemical testing and still remains 100% even after 40 000 s testing.

Combining with the theoretical calculations, the outstanding performance of the MG catalyst for HER can be attributed to the intrinsic chemical heterogeneity on the multicompositional disordered surface which provides abundant types of active site and the selective dealloying of elements which produces self-optimized active sites during the electrochemical cycling. Our study uncovers a new mechanism for improving the durability of catalysts and sheds some light on designing the non-noble metal catalysts with excellent performances.

Experimental Section

Experimental methods and any associated references can be found in the Supporting Information.

Supporting Information

Supporting Information is available from the Wiley Online Library or from the author.

Acknowledgements

[1] a) M. S. Dresselhaus, I. L. Thomas, *Nature* **2001**, *414*, 332; b) J. A. Turner, *Science* **2004**, *305*, 972; c) M. G. Walter, E. L. Warren, J. R. McKone, S. W. Boettcher, Q. Mi, E. A. Santori, N. S. Lewis, *Chem. Rev.* **2010**, *110*, 6446.

[2] J. Greeley, T. F. Jaramillo, J. Bonde, I. Chorkendorff, J. K. Norskov, *Nat. Mater.* **2006**, *5*, 909.

[3] Y. Jiao, Y. Zheng, M. Jaroniec, S. Z. Qiao, *Chem. Soc. Rev.* **2015**, *44*, 2060.

[4] D. Merki, X. Hu, *Energy Environ. Sci.* **2011**, *4*, 3878.

[5] a) H. W. Liang, S. Bruller, R. Dong, J. Zhang, X. Feng, K. Mullen, *Nat. Commun.* **2015**, *6*, 7992; b) M. R. Gao, J. X. Liang, Y. R. Zheng, Y. F. Xu, J. Jiang, Q. Gao, J. Li, S. H. Yu, *Nat. Commun.* **2015**, *6*, 5982.

[6] a) Y. Li, H. Wang, L. Xie, Y. Liang, G. Hong, H. Dai, *J. Am. Chem. Soc.* **2011**, *133*, 7296; b) J. Deng, P. Ren, D. Deng, X. Bao, *Angew. Chem., Int. Ed.* **2015**, *54*, 2100; c) X. Yan, L. Tian, M. He, X. Chen, *Nano Lett.* **2015**, *15*, 6015; d) M. Gong, W. Zhou, M. C. Tsai, J. Zhou, M. Guan, M. C. Lin, B. Zhang, Y. Hu, D. Y. Wang, J. Yang, S. J. Pennycook, B. J. Hwang, H. Dai, *Nat. Commun.* **2014**, *5*, 4695; e) W. F. Chen, J. T. Muckerman, E. Fujita, *Chem. Commun.* **2013**, *49*, 8896; f) J. S. Li, Y. Wang, C. H. Liu, S. L. Li, Y. G. Wang, L. Z. Dong, Z. H. Dai, Y. F. Li, Y. Q. Lan, *Nat. Commun.* **2016**, *7*, 11204.

[7] T. F. Jaramillo, K. P. Jørgensen, J. Bonde, J. H. Nielsen, S. Horch, I. Chorkendorff, *Science* **2007**, *317*, 100.

[8] G. Doubek, R. C. Sekol, J. Li, W.-H. Ryu, F. S. Gittleson, S. Nejati, E. Moy, C. Reid, M. Carmo, M. Linardi, P. Bordeenithikasem, E. Kinser, Y. Liu, X. Tong, C. O. Osuji, J. Schroers, S. Mukherjee, A. D. Taylor, *Adv. Mater.* **2015**, *28*, 1940.

[9] J. M. McEnaney, J. C. Crompton, J. F. Callejas, E. J. Popczun, A. J. Biacchi, N. S. Lewis, R. E. Schaak, *Chem. Mater.* **2014**, *26*, 4826.

[10] a) H. Vrubel, D. Merki, X. Hu, *Energy Environ. Sci.* **2012**, *5*, 6136; b) X. Ge, L. Chen, L. Zhang, Y. Wen, A. Hirata, M. Chen, *Adv. Mater.* **2014**, *26*, 3100.

[11] a) M. D. Demetriou, M. E. Launey, G. Garrett, J. P. Schramm, D. C. Hofmann, W. L. Johnson, R. O. Ritchie, *Nat. Mater.* **2011**, *10*, 123; b) M. W. Chen, *Annu. Rev. Mater. Res.* **2008**, *38*, 445.

[12] R. C. Sekol, G. Kumar, M. Carmo, F. Gittleson, N. Hardesty-Dyck, S. Mukherjee, J. Schroers, A. D. Taylor, *Small* **2013**, *9*, 2081.

[13] M. Carmo, R. C. Sekol, S. Ding, G. Kumar, J. Schroers, A. D. Taylor, *ACS Nano* **2011**, *5*, 2979.

[14] M. Zhao, K. Abe, S.-i. Yamaura, Y. Yamamoto, N. Asao, *Chem. Mater.* **2014**, *26*, 1056.

[15] Y. Yang, T. A. Maark, A. Peterson, S. Kumar, *Phys. Chem. Chem. Phys* **2015**, *17*, 1746.

[16] A. Inoue, N. Nishiyama, H. Kimura, *Mater. Trans., JIM* **1997**, *38*, 179.

[17] a) D. Voiry, H. Yamaguchi, J. Li, R. Silva, D. C. B. Alves, T. Fujita, M. Chen, T. Asefa, V. B. Shenoy, G. Eda, M. Chhowalla, *Nat. Mater.* **2013**, *12*, 850; b) A. Le Goff, V. Artero, B. Jousselme, P. D. Tran, N. Guillet, R. Métayé, A. Fihri, S. Palacin, M. Fontecave, *Science* **2009**, *326*, 1384; c) L. Liao, J. Zhu, X. Bian, L. Zhu, M. D. Scanlon, H. H. Girault, B. Liu, *Adv. Funct. Mater.* **2013**, *23*, 5326; d) S. Cobo, J. Heidkamp, P. A. Jacques, J. Fize, V. Fourmond, L. Guetaz, B. Jousselme, V. Ivanova, H. Dau, S. Palacin, M. Fontecave, V. Artero, *Nat. Mater.* **2012**, *11*, 802.

[18] J. Kibsgaard, T. F. Jaramillo, F. Besenbacher, *Nat. Chem.* **2014**, *6*, 248.

[19] Y. Zheng, Y. Jiao, Y. Zhu, L. H. Li, Y. Han, Y. Chen, A. Du, M. Jaroniec, S. Z. Qiao, *Nat. Commun.* **2014**, *5*, 3783.

[20] D. Merki, S. Fierro, H. Vrubel, X. Hu, *Chem. Sci.* **2011**, *2*, 1262.

[21] P. F. Guan, T. Fujita, A. Hirata, Y. H. Liu, M. W. Chen, *Phys. Rev. Lett.* **2012**, *108*, 175501.

[22] a) B. Hinnemann, P. G. Moses, J. Bonde, K. P. Jørgensen, J. H. Nielsen, S. Horch, I. Chorkendorff, J. K. Nørskov, *J. Am. Chem. Soc.* **2005**, *127*, 5308; b) J. K. Nørskov, T. Bligaard, A. Logadottir, J. Kitchin, J. Chen, S. Pandelov, U. Stimming, *J. Electrochem. Soc.* **2005**, *152*, J23; c) Y. Ito, W. Cong, T. Fujita, Z. Tang, M. W. Chen, *Angew. Chem., Int. Ed.* **2015**, *54*, 2131.

[23] A. Hirata, P. F. Guan, T. Fujita, Y. Hirotsu, A. Inoue, A. R. Yavari, T. Sakurai, M. W. Chen, *Nat. Mater.* **2011**, *10*, 28.